International Journal of Technology

http://ijtech.eng.ui.ac.id



Research Article

Kaolinite-Based Photocatalysts for Azo Dyes Degradation under Xenon and Sunlight Irradiations: The Effects of Electro-Deionization and Impregnation Methods

Khoirina Dwi Nugrahaningtyas ^{1,*}, IF Nurcahyo ¹, Desinta Yulyana Putri ¹, Sri Juari Santoso ², Eny Kusrini ^{3,4,**}, Anwar Usman ⁵, Lee D. Wilson ⁶

Abstract: Azo dyes pose a significant environmental concern due to their high stability and resistance to natural degradation. Therefore, this study aims to explore the use of kaolinite–based photocatalysts for azo dye degradation with methylene blue (MB) as an azo dye model. The transition metals–kaolinite composites (TMs-kaolinite) (where TM = Fe, Ni, or Zn) were prepared using 2 methods, namely electro-deionization (ED) and impregnation (IMP). The performance of TMs-kaolinite photocatalysts for azo dye degradation was evaluated using xenon and sunlight irradiations. The activities of degradation reaction of MB were observed by varying photocatalyst types, time of illumination, and type of irradiation. The most excellent photocatalytic activity for degradation of MB was Zn-Kaolinite IMP with an efficiency of 92% during 90 minutes of irradiation. Meanwhile, pristine kaolinite was the best adsorbent for the removal of MB without degradation process, with an adsorption efficiency of 98%. These results showed that TMs-kaolinite showed high photocatalytic activity for degradation of azo dye, with sunlight irradiation being more effective than xenon irradiation. Different forms of TMs-kaolinite catalysts had different phenomena and mechanisms for the photodegradation of MB. TMs in TMs-kaolinite played an important role in the performance of photocatalysts.

¹Department of Chemistry, Faculty of Mathematics and Natural Sciences, Sebelas Maret University, Jl. Ir Sutami No 36A, Surakarta, 57126, Indonesia

²Department of Chemistry, Faculty of Mathematics and Natural Sciences, Universitas Gadjah Mada, Sekip Utara PO BOX BLS 21 Yogyakarta 55281, Indonesia

³Department of Chemical Engineering, Faculty of Engineering, Universitas Indonesia, Kampus Baru UI, Depok 16424, Indonesia

⁴Research Group of Green Product and Fine Chemical Engineering, Laboratory of Chemical Product Engineering, Department of Chemical Engineering, Universitas Indonesia, Kampus Baru UI, Depok, 16424, Indonesia

⁵Department of Chemistry, Faculty of Science, Universiti Brunei Darussalam, Jalan Tungku Link, BE1410, Brunei Darussalam

⁶Department of Chemistry, University of Saskatchewan 110 Science Place, Room 156 Thorvaldson Building, Saskatoon, SK S7N 5C9, Canada

^{*}Corresponding author: khoirinadwi@staff.uns.ac.id, Tel.: +62271663375, Fax.: +62271663375

^{**} Corresponding author: eny.k@ui.ac.id, Tel.: +62217863516 ext. 204

The authors were grateful to the Legal Entity State Funding Assistance (BPPTNBH) under the Indonesian Collaboration Study Program (RKI) Scheme C [Decision Letter No. 767/UN27/HK/2023 and Contract No. 590.1/UN27.22/HK.07.00/2023]

Keywords: Azo dyes; Electro-Deionization and impregnation; Kaolinite; Photodegradation; Sunlight; Transition metals

1. Introduction

Rapid industrialization has increased pollution associated with wastewater discharge and exhaust emissions. These environmental contaminants can threaten human health and long-term development (Wang et al., 2022; Mousavi et al., 2016). One of the fastest-growing industries is the textile industry and its derivatives. Economic reasons and the lack of knowledge of business actors prevent waste processing from being carried out properly in the industry, leading to detrimental effects.

Azo dyes are widely used in the textile, leather, cosmetic, food, and paper sectors (Sudha and Saranya, 2014). When dumped into aquatic habitats, these dyes mix with water and enter the bodies of aquatic biota, resulting in bioaccumulation. Physically, azo dyes that enter the river cause coloration and block light from entering the water body, thereby affecting the photosynthesis process of phytoplankton or aquatic plants. Chemically, it can reduce oxygen levels in polluted waters and result in the death of aquatic biota. Azo dyes that degrade anaerobically in aquatic environments can yield hazardous aromatic amine compounds due to their high toxicity. An example of a compound formed in the anaerobic process is chloroaniline, which can harm human health as it affects the respiratory organs, urogenital organs, and causes nervous disorders (Santos et al., 2021). The complex aromatic structure of azo dyes makes it difficult to degrade by traditional biological processing processes (Wang et al., 2022). Therefore, there is a need for an effective processing method.

Dye degradation often uses photon energy, such as UV radiation or sunshine. In addition, sunlight has a higher intensity and longer wavelength (310–2300 nm) than UV light (200–380 nm). Sunlight is also a combination of approximately 45% visible light and approximately 3% UV light. This shows that sunlight has a relatively high energy and can provide a large amount of photon energy, leading to a better degradation process.

In recent years, catalysis and photocatalysis methods have been developed for environmental remediation due to their low cost, environmental friendliness, nontoxicity, and stability (Ramakrishna et al., 2022; Zyoud et al., 2019). One porous material widely used as catalyst and photocatalyst for dye waste processing is kaolinite (Kusrini et al., 2024; Ulfiati et al., 2022). This material is known for its layered and porous structure, which offers several advantages. In addition, it is non–corrosive, inexpensive, environmentally friendly, and abundant. The high surface area and the abundance of hydroxyl (OH) groups on Kaolin's surface contribute to its photocatalytic capabilities (Cao et al., 2021), in addition to its porous structures (Apriyanti et al., 2023).

Despite the potential, previous studies have found that kaolinite modified with metal can increase the efficiency of kaolinite photodegradation (da Trindade et al., 2024; Chen et al., 2023). Increasing photocatalytic efficiency can be achieved by designing the structure, doping metals or non–metals, heterojunctions, and surface modifications (Cao et al., 2021; Li et al., 2020). An effective method to increase the photocatalytic efficiency of clay is by converting it into a composite based on a combination of clay and semiconductors (Wongso et al., 2019; Zyoud et al., 2019; Janíková et al., 2017). This occurs because the semiconductors expand the clay absorption range of visible light waves, thereby increasing degradation rate of environmental organic pollutants. A previous study showed that Fe was more effective in upgrading the efficiency of clay in the photodegradation process for dye than Mn (Balarabe et al., 2022). Although Co metal was effective in photocatalytic applications, it is more expensive than Ni, Zn, and Fe (Türkyılmaz et al., 2017). These transition metals (TMs) in the form of oxides have low band gaps, specifically in Fe metal oxide (Fe₂O₃) of 2.2 eV, while Ni metal oxides (NiO) and Zn (ZnO) have band gaps of 3.6–4 eV and 3.37 eV, respectively (Da Trindade et al., 2019; Seo et al., 2019).

Several methods, such as impregnation (IMP) (Asmare et al., 2023), sol-gel (Shao et al., 2015), precipitation (Wongso et al., 2019), hydrothermal (Kutláková et al., 2015), and ion exchange,

(Hakimi et al., 2018) have been reported to synthesize metal-kaolinite composites. Among these methods, most are relatively complicated because their preparation comprises many steps, are less efficient, and require high energy, except IMP, which is a simpler method. IMP process requires modifying a support material by filling its pores with an active metal solution through immersion (Aviantara et al., 2024; Heriyanto et al., 2023; Nugrahaningtyas et al., 2022). Meanwhile, a new method, known as electro-deionization (ED), has been proposed to enhance the synthesis of metalkaolite composites. This method combines ion exchange with electrolysis system. ED is efficient because it is simple, easy to prepare with safe precursors, and optimal for balancing cations. The principle is based on the exchange of ion metals by using the difference in electrical potential in the transport of ions (Li et al., 2019; Pal et al., 2016). Therefore, this study aims to compare the effect of IMP and ED methods on the characteristics of transition metals-kaolinite composites (TMskaolinite) catalysts. Methylene blue (MB) was selected as a model azo dye to test the periodicity of TMs Fe, Ni, and Zn combined with kaolinite. Previous studies showed a relationship between the periodic properties of elements and their catalytic properties (Nugrahaningtyas et al., 2025; 2022). The photocatalytic degradation of MB using material has been reported, such as TiO2 (Suhaimi et al., 2022; Zulmajdi et al., 2019), kaolin-titania (Kamaluddin et al., 2021), and samarium complexes with 2,6-Naphtalenedicarboxylate ligand (Wulandari et al., 2019). Different forms of composites have different phenomena and mechanisms for the photodegradation of MB. Consequently, the current study is important to evaluate the different methods and the effect of TMs in forming (TMskaolinite) catalysts, aiming at the synergy between photoactivity of kaolinite and visible light absorption of transition metals (Zagloel et al., 2024). Various material engineering has been carried out to obtain the best physical, chemical, and biological properties for future material use, specifically as photocatalyst material. A UV-Vis was used to quantify the precise concentration of the MB solution post-degradation.

2. Methods

2.1. Materials and Instruments

The Ni(NO₃)₂, Zn(NO₃)₂, or Fe(NO₃)₃ salts with a pro–analysis grade were obtained from Merck (Germany), while the metal electrodes and ED tool kit were purchased from Edulab. The instruments used to characterize catalyst samples were Scanning Electron Microscope (SEM) (JEOL JSM 6510 LA) equipped with EDAX APEX, X-ray fluorescence spectrometry (Ranger BRUKER S2 puma), X-ray diffractometer (Shimadzu 7000) with Cu-K α radiation (λ = 1.540 Å), infrared spectrophotometer (FTIR Spectrophotometer, Shimadzu 8201 PC), and gas sorption analyzer (Quantachrome St. 3 on Nova Touch 4LX). Analysis of dye concentration was conducted using UV Vis (Double Beam Spectrophotometer HITACHI UH5300).

2.2. Preparation of TMs@kaolinite by ED Method

The salt bridge from kaolinite was made into pellets by pressing with filter paper on both sides, 3 cm long and 22.5 cm in diameter, then placed in an ED circuit device. Subsequently, the 2 pure metal electrodes (Ni, Zn, or Fe) were placed alternately in each container on the device. Electrodes were made with a length of 7.5 cm and a width of 1.6 cm, and the ED circuit was inserted into the Ni(NO₃)₂, Zn(NO₃)₂, or Fe(NO₃)₃ solutions alternately. Furthermore, electrolyte solution was made to a concentration of 0.1 M, while electro–ion exchange process used a voltage of 28.4 V and a current of 0.01 A for 3 hours. After the process was completed, it was washed with sufficient demineralization water. TMs@kaolinite was placed in an oven at 110°C for 3 hours, then calcined with air at 500°C for 3 hours, and the catalyst obtained was called TMs@kaolinite ED. The samples were characterized using XRD, FTIR, XRF, SEM, and SAA to determine the metals' nature, character, and content.

2.3. Preparation of TMs@kaolinite IMP Method

IMP method of catalyst preparation followed a modified version of an earlier procedure (Asmare et al., 2023; Nugrahaningtyas et al., 2022). A total of 100 milliliters of demineralization

water were used to make a suspension of kaolinite, stirring at room temperature for 30 minutes at 900 rpm. The suspension was filtered and mixed with electrolyte solution (Ni $(NO_3)_2$, Zn $(NO_3)_2$, or Fe $(NO_3)_3$) made to a concentration of 0.1 M. Furthermore, IMP process was carried out in 2 stages. The first stage lasted 16 hours at 30°C, while the second stage took 4 hours at 80°C. After IMP, the catalyst was dried and calcined for 3 hours at 500°C. XRD, FTIR, XRF, SEM, and SAA were used to evaluate the type, character, and content of metal ions in TMs@kaolinite.

2.4. Characterizations

In this study, the morphology and size of the monoliths were studied with SEM. The elemental composition was analyzed using X-ray fluorescence spectrometry. An X-ray diffractometer (Shimadzu 7000) was used for diffraction pattern and phase composition analysis. The functional groups of photocatalysts were detected using an infrared spectrophotometer (FTIR Spectrophotometer, Shimadzu 8201 PC). Furthermore, the catalyst's pore size and BET surface area were obtained from a gas sorption analyzer (Quantachrome St. 3 on Nova Touch 4LX). Analysis of dye concentration before and after testing was carried out using UV Vis spectrophotometer.

2.5. Photocatalytic Activity Test of Azo Dyes

The previous method was adjusted to measure the samples' photocatalytic activity (Setiadi et al. 2023). Methylene Blue, which was selected as a model of Azo dye, was dissolved in demineralization water until a solution of 1000 ppm was obtained. A photocatalytic test was performed on TMs@kaolinite without light, with artificial irradiation, and with natural sunlight.

The photocatalytic test without light (dark) was investigated by adding 0.1 g of TMs@kaolinite into 100 mL of 20 ppm MB and stirring at 600 rpm for 90 minutes. After 30 minutes, every 10 minutes, the solution was carefully taken using a syringe equipped with a filter (0.22 μ m) and analyzed for absorbance using UV–Vis as the concentration of MB remaining in the solution. The concentration of MB was calculated using a standard curve. Subsequently, the adsorption efficiency was calculated using Equation 1.

Adsorption efficieny =
$$\frac{[MB]_{initial} - [MB]_{final}}{[MB]_{initial}} \times 100\%$$
 (1)

Where [MB] denoted the concentration of Methylene blue.

A similar procedure was used to perform the photocatalytic test under a xenon lamp (Michiba H1 Xenon white 5000k Bohlam Mobil Halogen 55 W – 12 V) as an artificial lighting resource. First, to homogenize the suspension, 0.1 g of TMs@kaolinite was added to 100 mL of 20 ppm MB and stirred at 600 rpm for 30 minutes in the dark. After this procedure, the photodegradation test was continued by artificially irradiating a xenon lamp for 1 hour, stirring at 600 rpm. Every 10 minutes, the solution was carefully taken using a syringe equipped with a filter (0.22 μ m), and its absorbance was analyzed using UV-Vis.

2.6. The adsorption kinetic modeling

Pseudo-first-order (PFO) and pseudo-second-order (PSO) kinetic models were used to calculate the kinetics of MB removal in this study (Tsaviv et al., 2024; Darmadi et al., 2023). Based on the linear regression form of PFO and PSO, the reaction order was determined based on the correlation value (R²).

3. Results and Discussion

3.1. SEM studies

The structure of pristine kaolinite showed a flat plate—like shape that was stacked and arranged in layers and regularly (See S1). These layers were connected through hydrogen bonds, contributing to kaolinite's unique structure and characteristics (Ivanić et al., 2015). Through chemical or physical modification, the surface and pores could be altered better to support the placement and reaction of photocatalyst particles. This modification improved the interaction between the photocatalyst

and the substrate, increasing the efficiency of the photochemical reaction. Although kaolinite was not a natural semiconductor, this modification allowed kaolinite to act as an effective media support in photocatalytic reactions.

Adding metal to kaolinite caused the distance between the layers to widen, showing that the metal had succeeded in inserting itself between kaolinite layers. The TMs@kaolinite showed damage in several parts, decreased regularity, and widening of the interlayer distance compared to kaolinite (See S2–S7). This phenomenon, due to Ni, Zn, and Fe metal particles, could disrupt hydrogen bonds between layers, causing changes in the structure of kaolinite. The larger size of the metal particles compared to the interlayer space of kaolinite caused binding to kaolinite surface penetrating the interlayer space, damaging kaolinite sheet. These structural changes could increase particle reactivity because larger particles had a higher surface area and more active reaction sites (Nugrahaningtyas et al., 2025; Ramadji et al., 2022; Yahaya et al., 2017).

Several differences were observed in structural changes between the ED and IMP methods. In the IMP method, the layers were still visible because only metal insertion widened the distance between layers. However, in the ED method, there was a change of ions that greatly changed the crystal structure. The layer structure of the TMs@kaolinite ED appeared damaged due to overlapping or collapse between kaolinite layers. Furthermore, there could have been coagulation in the pores of kaolinite layer, which occurred during a less—than—optimal calcination process. These structural characteristics not only increased the specific surface area but also increased the porosity ratio. Therefore, both methods significantly improved the surface properties of pristine kaolinite, which caused partial irregularities in particle shape and reduced crystal regularity on kaolinite surface.

After IMP, the clay morphology showed that the layers were uneven and irregular due to TMs's coating of kaolinite surface (See S5–S7). The EDX data confirmed the results of investigations, which detected the presence of SiO_2 , Al_2O_3 , and the metals Ni, Zn, and Fe. Furthermore, the Fe/kaolinite IMP had the greatest metal content at 5.71% loading. This data suggested that the IMP procedure successfully incorporated more Fe metal into kaolinite.

3.2. XRD studies

TMs@kaolinite ED showed that most metals were successfully embedded in kaolinite. Analysis using XRD showed that the addition of metal damaged the main structure of kaolinite (Figure 1).

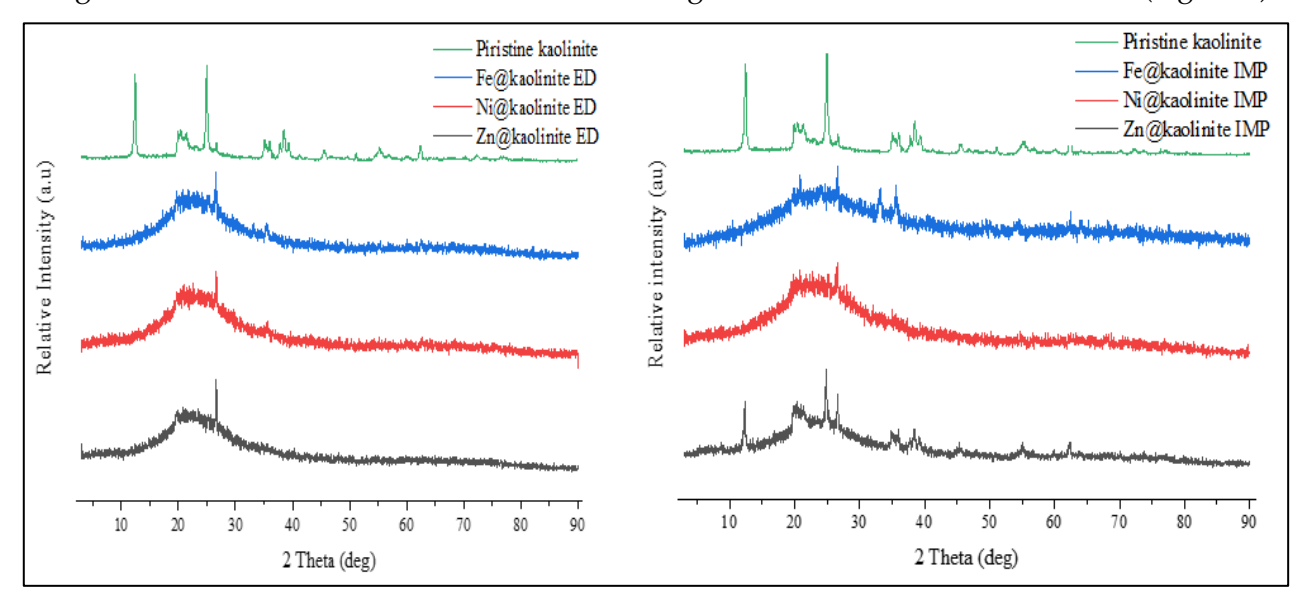


Figure 1 Comparison of the XRD patterns of pristine kaolinite and TMs@kaolinite by ED and IMP methods

The investigation showed that kaolinite used in this investigation was that with formula $Al_2(Si_2O_5)$ (OH)₄, the ICDD # 00-079-1570, with 100% purity. In this study, the diffraction pattern for TMS@kaolinite also confirmed the presence of kaolinite (ICDD # 00-002-0105) as the main phase. The peak shift at 20 of approximately 25° was possible due to changes in basal spacing during metal loading between layers of kaolinite. The results showed that the pristine kaolinite conformed to the ICDD standard pattern number 01-079-1570, with typical diffraction peaks appearing at 20 = 12.4°, 19.8°, 21.2°, and 24.9°. Furthermore, the 20 value correlated with d–spacing and Miller indexes, respectively, such as 7.09 Å (d_{010}); 4.44 Å (d_{020}); 4.17 Å (d_{111}); and 3.56 Å (d_{002}), which were the main typical diffraction patterns of kaolinite. The pristine kaolinite also contained quartz (SiO₂) as impurities, which were shown at 20 = 20.5°, 26.69°, and 39.31° based on the ICDD standard #00–046–1045 (Hariyanto et al., 2021; Beddiaf et al., 2015).

Interpretation of the TMs@kaolinite diffraction pattern showed that adding metal caused an intensity decrease and a shift in the typical diffraction peak towards a small angle. The decrease in the intensity of the typical kaolinite diffraction peak showed a reduction in kaolinite's crystallinity. Meanwhile, the shift in the 2θ value towards a smaller direction showed that the distance between layers was getting wider with the presence of metal. An in–depth analysis of the TMs@kaolinite diffraction pattern showed new peaks compared to the pristine diffraction pattern.

Further analysis observed that the hematite and magnetite phases were confirmed for Fe@kaolinite ED and Fe@kaolinite IMP, referring to ICDD# 00-072-0469 and 00-076-0958. In this study, the 2θ at 62.78° of Ni@kaolinite ED showed the presence of nickel oxide (NiO) with d-spacing 1.37 Å (d_{220}) following #ICDD 00-044-1159 (Mustapha et al., 2020). The ED process caused some of the silica in Ni@kaolinite ED to decay and form silica dioxide (ICDD # 00-077-1060). Meanwhile, nickel was present in the dwornikite phase for Ni@kaolinite IMP, corresponding to ICDD reference #00-081-0021. Zn metal was present in both the Zn@kaolinite as zinc oxide sulfate and zinc hydroxide phases under ICDD # 00-03201475 and ICDD # 00-074-0094 (Hamrayev and Shameli, 2022).

3.3. FTIR studies

The FTIR spectra of kaolinite showed the presence of 4 characteristic bands in the form of sharp absorptions at 3621, 3656, 3671, and 3696 cm⁻¹. This originated from the stretching vibration mode of the –OH function series bound to the octahedral Al atom (Al–OH) from the surface or interlayer of kaolinite (see Figure 2). The absorption bands at 3621 and 3671 cm⁻¹ were caused by the inner hydroxyl (–OH) stretching region (Majid et al., 2023; Maged et al., 2020). Meanwhile, the Al–OH bond also appeared at 3656 cm⁻¹ as an octahedral structure. The Al–OH vibration caused by the alumina kaolinite sheets in coordination with the OH group was properly shown by the peaks at 913 and 3696 cm⁻¹ (Wang et al., 2021; Wongso et al., 2019). The varied intensity of this band was due to the disruption of the hydroxyl through the formation of hydrogen bonds with TMs (Wang et al., 2021). Both metal addition methods showed that absorption at wavenumbers around 3600 to 3750 cm⁻¹ was significantly reduced after metal addition. A strong suspicion that ion exchange occurs between protons and metal ions was observed. The characteristic peaks mostly disappeared in the TMs@kaolinite, also showing the destruction of the octahedral sheets of Al–OH due to the calcination treatment (Wongso et al., 2019).

A peak appeared around 3400 cm⁻¹ in TMs@kaolinite, showing the stretching vibration of hydroxyl (Al–OH or Si–OH). The absorption around 3400 and 1639 cm⁻¹ could also be attributed to the stretching and bending vibrations of H–O–H of the adsorbed water, respectively. The hydroxyl deformation of the water molecules caused a small peak at 2350 cm⁻¹ in TMs@kaolinite IMP. A weak peak at 2923 cm⁻¹ in TMs@kaolinite ED was from stretching aliphatic hydrocarbons, showing the presence of organic impurities, although their presence was insignificant due to beneficiation.

Tree peaks at around 1000 cm⁻¹ corresponded to the stretching vibrations of silicon monoxide (Si–O), O–Si–O, and O–Al–O. The presence of silicon monoxide was associated with the symmetric

stretching vibrations of quartz, showing that silicon oxide was predominantly in kaolinite and TMs@kaolinite. Meanwhile, the appearance of O–Si–O and O–Al–O was from asymmetric stretching of the aluminosilicate framework (Kusrini et al., 2024). The TMs@kaolinite ED spectra showed a red shift in the asymmetric stretch of the aluminosilicate framework from 1115 cm⁻¹ to 1076 cm⁻¹ for Ni@kaolinite ED, Zn@kaolinite ED, and Fe@kaolinite ED. In this study, the Ni@kaolinite IMP experienced a redshift to 1084 cm⁻¹, and Zn@kaolinite IMP showed a shift to 1037 cm⁻¹. The red shift showed that the presence of metal weakened the Si–O–S and Si–O–Al bonds. A different phenomenon occurred in Fe@kaolinite IMP, whose absorption wavenumber became higher (blue shift), which was 1169 cm⁻¹. According to previous studies, the blue shift occurred due to the de–alumination process or releasing Al in kaolinite structure to Al outside the framework (Holmberg et al., 2004). The de–alumination process caused a reduction in the amount of Al and raised its spacing. Consequently, the blue shift was due to the shortening of the Si–O–Si or Si–O–Al bonds (Zhang et al., 2024; Nugrahaningtyas et al., 2021).

In the Zn@kaolinite IMP catalyst, the peak at 915 cm⁻¹ was still visible, which was the Al–OH functional group in the bending mode, while in other catalysts, there was none. Therefore, it could be concluded that adding Zn metal to kaolinite did not change kaolinite framework. The small peak at 794 cm⁻¹ was caused by metal impurities bound to aluminum and hydroxyl vibrations. Furthermore, the adsorption band of the M–O functional group (Al–O or Si–O) correlated with wave numbers 684, 534, and 469 cm⁻¹, showing the presence of the Si–O functional group but in a different environment. The band at wave number 684 cm⁻¹ showed stretching vibration in Si–O, and the sharp and clear peak around 534 cm⁻¹ corresponded to the bending vibration of Si–O–Al, showing that besides silica oxide, the sample also contained aluminum oxide.

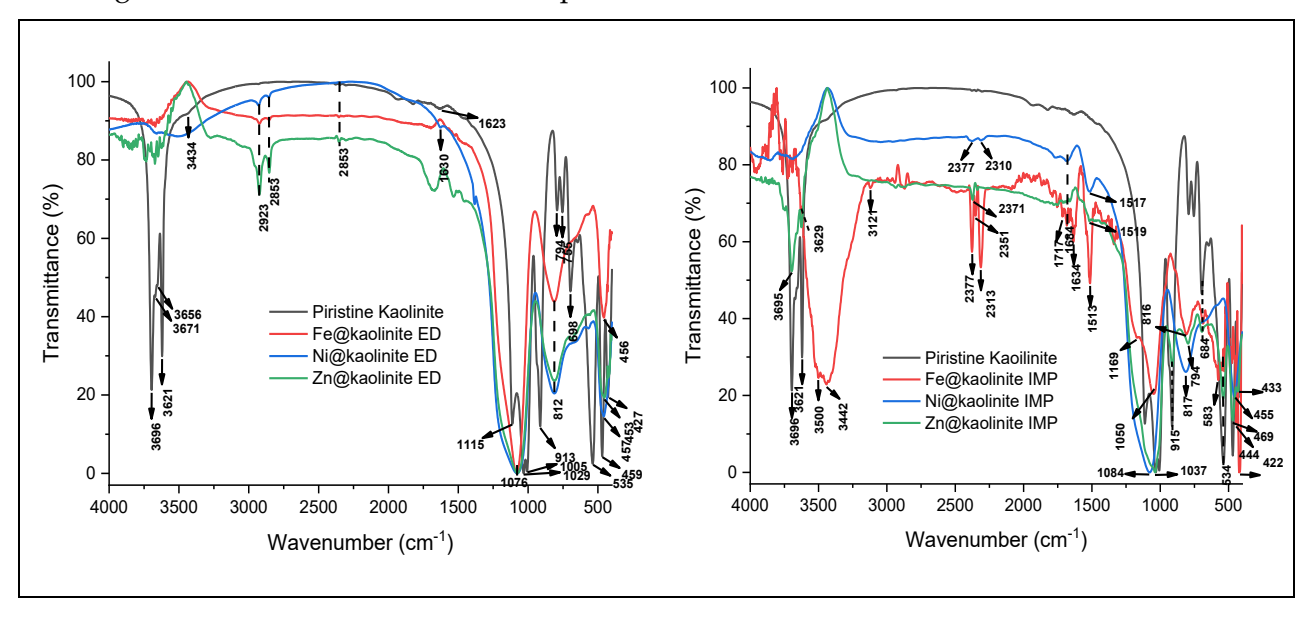


Figure 2 FTIR spectra of pristine kaolinite and TMs@kaolinite photocatalysts by ED and IMP methods

The presence of metal of TMs@kaolinite ED was shown by absorption peaks at 457, 453, and 456 cm⁻¹, respectively. Meanwhile, TMs@kaolinite IMP had absorption peaks at 433, 433, and 422 cm⁻¹, respectively. The vibrations at 457 and 433 cm⁻¹ showed the presence of Ni–O from the NiO compound. In this study, the adsorption band at 453 and 433 cm⁻¹ was from Zn–O functional groups, while that at 456 and 422 cm⁻¹ was from Fe–O functional groups compound due to the oxidation process of the Fe–produced Fe₂O₃ compound.

The Zn@kaolinite IMP and Fe@kaolinite IMP spectra showed absorption at 534 and 583 cm⁻¹ from a Si–O functional group bound to the Al atom (Si–O–Al). This proved that the calcination process at a temperature of 500°C could reduce –OH with the loss of water bound to the crystal

lattice and change the metal into a metal oxide that replaced the –OH group. The addition of metal by IMP methods did not damage its main structure. Therefore, IMP method was better at producing TMs@kaolinite catalysts without damaging the main structure of kaolinite. In this case, its photocatalytic properties could also increase.

3.4. Adsorption-desorption isotherm analysis

Adsorption—desorption isotherm analysis was conducted to determine the catalyst synthesis material's surface area characteristics, pore size, and pore volume (Figure 3). The BET, BJH, and t-plot methods were used to calculate the specific surface area, the pore diameter, and the pore volume. Furthermore, the adsorption isotherms of TMs@kaolinite and kaolinite followed the type III isotherm model of Brauneur, Deming, and Teller (BDDT). This model showed a system characterized by mesoporous dimensions and monolayer behavior. The presence of a hysteresis loop in the adsorption isotherm was typical of mesopores. Adsorption on the mesopore surface promoted the formation of multilayers, which caused capillary condensation. Therefore, the catalyst exhibited adsorption behavior similar to macropores at low pressures but was then followed by a significant increase in adsorption at higher pressures. This was due to the capillary condensation inside the mesopores. The process of capillary condensation and evaporation at various relative pressures produced a hysteresis loop.

Textural analysis of kaolinite and TMs@kaolinite showed that the surface area of pristine kaolinite increased in the presence of metal (Table 1). The surface area of the TMs@kaolinite IMP tended to be larger than that of TMs@kaolinite ED. A wider surface area promised more active sites for both adsorption and photodegradation. Meanwhile, kaolin's surface area decreased significantly after adding Ni and Zn metals using the ED method. The decrease in catalyst surface area was thought to be caused by the coagulation of Ni and Zn metals on the surface of the Kaolin catalyst, thereby closing the pores of the Kaolin and reducing the surface area of contact between the catalyst's active site and the reactants.

The IMP method produced a catalyst with a smaller average pore radius than the ED method. Meanwhile, the average pore radius reduction showed that some metal particles entered the pores of kaolinite, as a result, the metal particles blocked the pores. The pristine kaolinite and TMs@kaolinite samples had an average pore size of more than 60 Å. Consequently, it was classified in the mesoporous region. The Fe@kaolinite IMP had the highest surface area ($15.867 \text{ m}^2/\text{g}$), while the Zn@kaolinite IMP had the 2^{nd} largest surface area ($12.512 \text{ m}^2/\text{g}$). Adding the TMs in kaolinite had little impact on the increasing surface area.

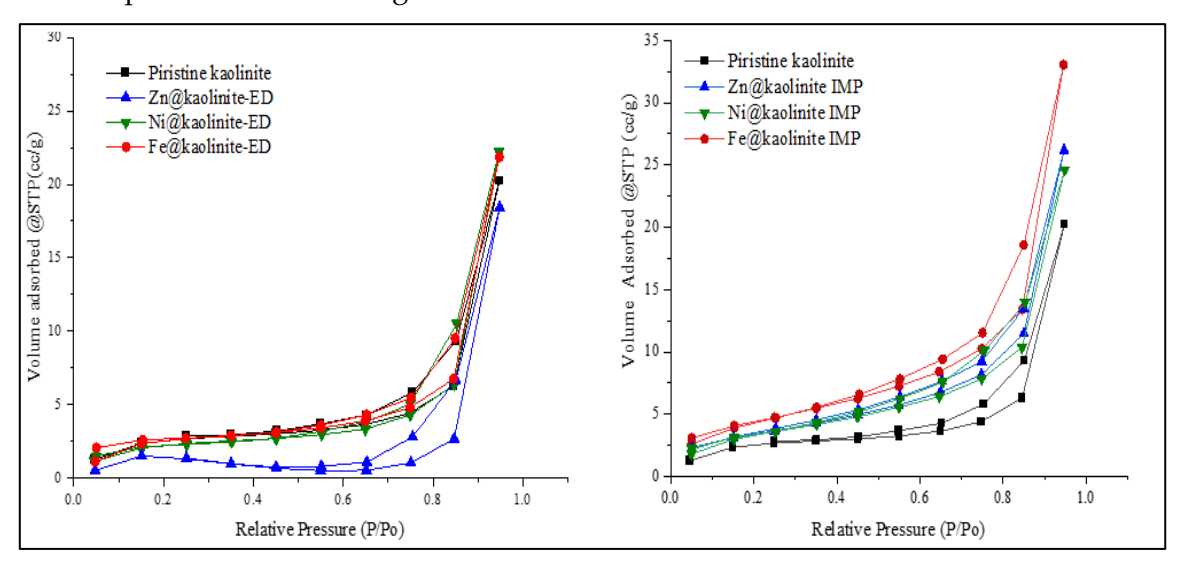


Figure 3 Adsorption and desorption isotherm profiles of pristine kaolinite and TMs@kaolinite photocatalyst by ED and IMP methods

Table 1 Comparison of the Specific Surface Area, Total Pore Volume, and Average Pore Radius of Catalyst

Sample	Specific Surface Area (m²/g)	Total Volume Pore (x10 ⁻² cc/g)	Average Pore Radius (Å)
Piristine kaolinite	8.334	3.138	73
Fe@kaolinite ED	8.989	3.389	75
Ni@kaolinite ED	7.615	3.448	91
Zn@kaolinite ED	2.948	2.855	194
Fe@kaolinite IMP	15.867	5.122	65
Ni@kaolinite IMP	12.174	3.815	63
Zn@kaolinite IMP	12.512	4.059	65

3.5. The Photocatalytic Activity

Without a catalyst, the maximum degradation efficiency of methylene blue (MB) reached 22% after 1 hour of irradiation. The dye degraded even without a catalyst because the chromophore group absorbed photons. The absorbed energy could break the bonds in the chromophore region of the dye, breaking it down into smaller molecules, which then break down further into simple compounds (Groeneveld et al., 2023). The catalyst sample had a higher efficiency of MB degradation because the metal was a semiconductor, while kaolinite was not. Therefore, the TMs@kaolinite catalyst absorbed light more efficiently.

3.6. The effects of time in photodegradation of MB

In this study, 4 key elements were required for catalytic photodegradation, namely a light energy source (photons), a specific compound to be degraded, oxygen as an oxidant, and photocatalyst. Xenon lamps and sunlight were known to have visible light spectra. The dye model used was methylene blue in aqueous media as the target compound to be degraded. At the same time, air, as a source of oxygen, was electron acceptor and photocatalyst made of TMs@kaolinite.

Photodegradation of MB using a TMs@kaolinite photocatalyst was conducted in a controlled process. Stirring was carried out during irradiation to ensure uniformity in the photodegradation reaction and even dispersion of the TMS@kaolinite photocatalyst in methylene blue. Irradiation was performed several times to study the photocatalytic activity as a function of time (Figure 4). The decrease in methylene blue concentration due to adsorption events that could accompany the photodegradation reaction was also measured as a correction factor for the photocatalytic properties of TMs@kaolinite. Based on the study results, it could be predicted whether methylene blue was only adsorbed or underwent adsorption and degradation processes simultaneously facilitated by the TMs@kaolinite photocatalyst.

After an hour of exposure, there was no present MB photodegradation without a catalyst. The dye degraded even without a catalyst because the chromophore group absorbed photons. In this study, the absorbed energy could break the bonds in the chromophore region of the dye, breaking it down into smaller molecules, which then break down further into simple compounds (Groeneveld et al., 2023). The catalyst sample had a higher efficiency of dye degradation because the metal was a semiconductor, while kaolinite was not. Adding metal to kaolinite showed an increase in the efficiency of photodegradation of MB compared to kaolinite without metal. These results showed that the photocatalytic activity of MB degradation was effectively increased in the presence of metals. Therefore, the TMs@kaolinite catalyst absorbed light more efficiently. The highest degradation efficiency was achieved using Zn@kaolinite. Degradation efficiency for MB reached 92% after exposure for 60 minutes under natural sunlight. Furthermore, the photodegradation efficiency in this study was higher compared to previous reports, which used a GMC-Fe (Graphitic mesoporous carbon) catalyst under UV light (Ulfa et al., 2023).

Similar studies related to the photocatalytic degradation of MB used TiO₂ (Suhaimi et al., 2022; Zulmajdi et al., 2019), kaolin-titania (Kamaluddin et al., 2021) and samarium complexes with 2,6-Naphtalenedicarboxylate ligand (Wulandari et al., 2019). Meanwhile, the removal of MB from an

aqueous solution using pectin-alginate-titania composite microparticles had been reported by (Zamri et al., 2021). A similar study for the removal of MB using durian rind was also evaluated by Asbollah and coworkers (Asbollah et al., 2021). According to the previous report, different forms of catalysts or composites had different phenomena and mechanisms for the photodegradation of MB.

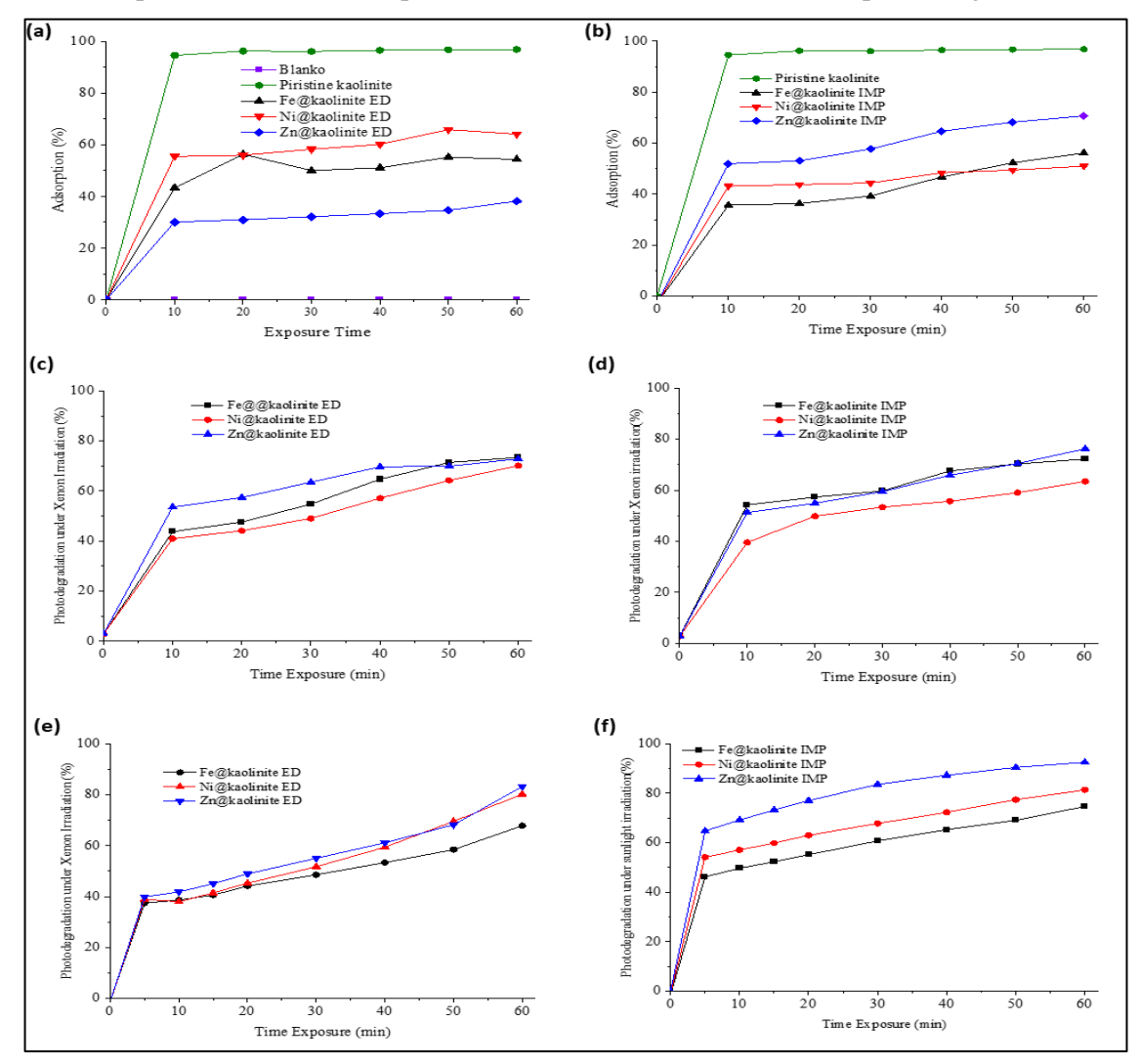


Figure 4 The impact of exposure duration on the adsorption and photodegradation efficiency of MB

The TMs played an important role in the performance of the TMs-kaolinite catalysts for the photodegradation of MB. Zn-Kaolinite IMP catalyst was found to be the most excellent photocatalytic activity with efficiency photodegradation of 92% during 90 minutes of irradiation, even though it only exhibited the 2nd largest surface area (12.512 m²/g). Meanwhile, the rest of the TMs including Fe and Ni, had photodegradation efficiencies less than those of the Zn modifier (See Figure 5).

3.7. The Adsorption Kinetics

In this study, data analysis steps were conducted systematically better to understand MB absorption kinetics (Figure 5). The first step was to convert the liquid concentration data into the amount of MB absorbed, expressed in qt. These raw data were then plotted in a graph of qt against time (t) to visualize the absorption pattern. Furthermore, data fitting was performed using the asymptotic exponential equation. This equation was used to represent the raw data to facilitate further analysis. The asymptotic exponential equation could calculate a time of less than 10 minutes.

This equation also allowed the determination of the amount of MB absorbed at equilibrium conditions (qe), which was an important parameter in the adsorption kinetic analysis.

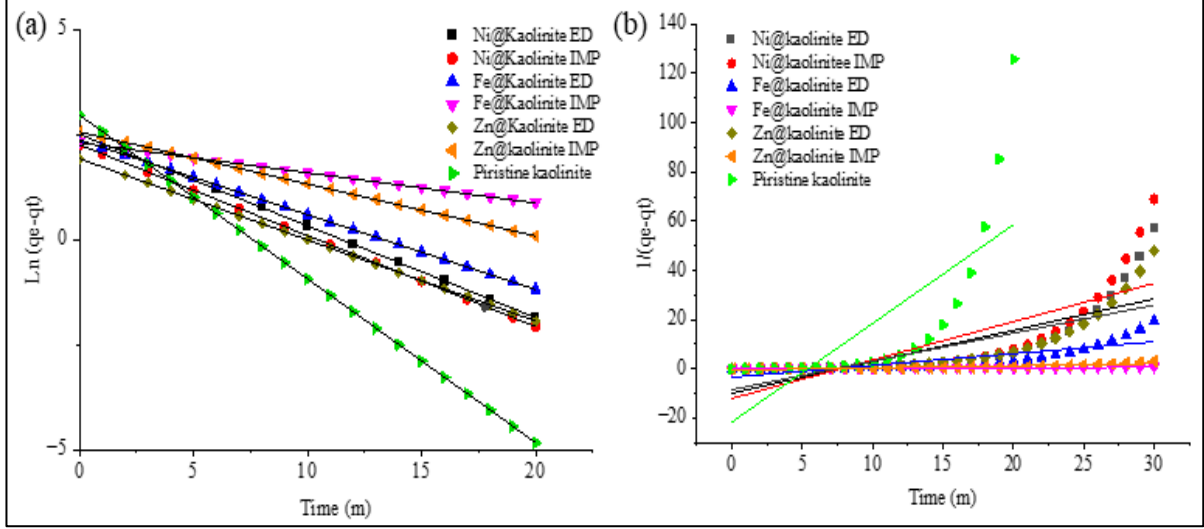


Figure 5 The adsorption kinetics data of MB fitted with (a) pseudo-first-order kinetic model and (b) pseudo-second-order kinetic model

The adsorption kinetics data of MB were evaluated using the pseudo-first-order and pseudo-second-order kinetic models (See Table 2). In this study, the asymptotic exponential equation produced data points (qt, t), which were then processed to obtain qe and qt values. This method provided a strong basis for quantitatively analyzing the kinetic mechanism of MB removal. Based on the results of this study, the MB removal of pristine kaolinite and TMs@kaolinite followed pseudo-first-order kinetics with an R²-value approaching 1.

Table 2 Parameter of adsorption kinetics, where * = multiple (x)

Sample	Pseudo-first-order equation		Pseudo-second-order equation			
		k				
	Ln (qe-qt) = -kt + ln qe	\mathbb{R}^2	(min ⁻¹)	1/(qe-qt) = k*t + 1/qe	R ²	
Piristine kaolinite	Ln(qe-qt) = -0.38976*t + 2.96034	1	0.39	1/(qe-qt) = 187.26*t-1226.5	0.616	
Ni@kaolinite ED	Ln(qe-qt) = -0.21812*t+2.5046	1	0.218	1/(qe-qt) = 68*t - 864.9	0.510	
Ni@kaolinite IMP	Ln(qe-qt) = -0.21625*t+2.25424	1	0.216	1/(qe-qt) = 79.7*t -1012.2	0.512	
Fe@kaolinite ED	Ln(qe-qt) = -0.17799*t+2.37235	1	0.18	1/(qe-qt) = 10.79*t-132.78	0.554	
Fe@kaolinite IMP	Ln(qe-qt) = -0.07114*t+2.29386	1	0.071	1/(qe-qt) = 0.06*t-0.44	0.814	
				1/(qe-qt) =		
Zn@kaolinite ED	Ln(qe-qt) = -0.19308*t+1.9204	1	0.19	35.563*t-443.983	0.535	
Zn@kaolinite						
IMP	Ln(qe-qt) = -0.12375*t+2.55671	1	0.124	1/(qe-qt) = 0.6361*t-7.05	0.653	

This study was comparable with the Lagergren pseudo-first-order result reported by Asbollah and colleagues with the R-value of 0.997 (Asbollah et al., 2021), although the photocatalytic degradation of MB on TMs@kaolinite may likely be multistep (Madani et al., 2024). Meanwhile, pristine kaolinite had the highest MB removal rate constant compared to TMs@kaolinite. The MB removal of pristine kaolinite was the fastest compared to TMs@kaolinite (see Table 2). This study's results showed that the kinetic parameters of TMs were not significantly influenced by their periodic characteristics.

4. Conclusions

In conclusion, the photocatalytic activity of pristine kaolinite and its composites (TMs@kaolinite) to degrade methylene blue (MB) under sunlight or xenon irradiation had been investigated. In this study, TMs@kaolinite photocatalysts were successfully prepared using ED and IMP methods to form metal oxides on the kaolin surface. Kaolinite only showed the removal of MB without degradation process with an adsorption efficiency of 98%. Furthermore, the presence of TMs in TMs-kaolinite catalysts played an important role in the performance of photocatalysts. The Zn@kaolinite IMP was the most effective catalyst in the photodegradation process of azo dyes under sunlight irradiation, with an efficiency of 92%. All of the adsorption kinetics adhered to the pseudo–first–order model. Furthermore, it was discovered that sunlight outperformed xenon lamps for MB photodegradation. In future studies, the different TMs and preparation methods for photocatalysts could be further evaluated to obtain the optimum for degradation of azo dye. This could be useful for practical in industries or mitigation of climate change and environmentally friendly.

Acknowledgements

The authors are grateful to thank Universitas Sebelas Maret for paying of the Article Processing Charge (APC) for this publication.

Author Contributions

KDN – conceptualization, supervision and analysis; IFN – Analysis, writing & review; DYP – Experiment & Investigation; SJS – Review; EK – Analysis, writing & review; AU – Editing & review; LDW – Review.

Conflict of Interest

The authors declare no conflicts of interest.

References

Apriyanti, E, Susanto, H & Widiasa, IN 2023, 'Preparation and performance evaluation of TiO₂ incorporated fly ash–kaolin ceramic membrane for oil/water separation', *International Journal of Technology*, vol. 15, no. 6, pp. 1959–1970, https://doi.org/10.14716/ijtech.v15i6.6294

Asbollah, MA, Mahadi, AH, Kusrini, E & Usman, A 2021, 'Synergistic effect in concurrent removal of toxic methylene blue and acid red–1 dyes from aqueous solution by durian rind: Kinetics, isotherm, thermodynamics, and mechanism', *International Journal of Phytoremediation*, vol. 23, no. 13, pp. 1432–1443, https://doi.org/10.1080/15226514.2021.1901851

Asmare, ZG, Aragaw, BA, Atlabachew, M & Wubieneh, TA 2023, 'Kaolin-supported silver nanoparticles as an effective catalyst for the removal of methylene blue dye from aqueous solutions', *ACS Omega*, vol. 8, no. 1, pp. 480–491, https://doi.org/10.1021/acsomega.2c05265

Aviantara, DB, Suciati, F, Hadiko, G, Indrasti, NS & Yani, M 2024, 'Microwave–assisted impregnation of zinc metal ions on surface of quenched pulverized shrimp shell waste', *International Journal of Technology*, vol. 15, no. 6, pp. 1946–1958, https://doi.org/10.14716/ijtech.v15i6.6170

Balarabe, BY, Bowmik, S, Ghosh, A & Maity, P 2022, 'Photocatalytic dye degradation by magnetic XFe₂O₃ (X: Co, Zn, Cr, Sr, Ni, Cu, Ba, Bi, and Mn) nanocomposites under visible light: A cost efficiency comparison', *Journal of Magnetism and Magnetic Materials*, vol. 562, article 169823, https://doi.org/10.1016/j.jmmm.2022.169823

Beddiaf, S, Chihi, S & Leghrieb, Y 2015, 'The determination of some crystallographic parameters of quartz, in the sand dunes of Ouargla, Algeria', *Journal of African Earth Sciences*, vol. 106, pp. 129–133, https://doi.org/10.1016/j.jafrearsci.2015.03.014

Cao, Z, Wang, Q & Cheng, H 2021, 'Recent advances in kaolinite-based material for photocatalysts', *Chinese Chemical Letters*, vol. 32, no. 9, pp. 2617–2628, https://doi.org/10.1016/j.cclet.2021.01.009

Chen, M, Yang, T, Han, J, Zhao, L, Zhao, J, Li, R, Huang, Y, Gu, Z & Wu, J 2023, 'The application of mineral kaolinite for environment decontamination: A review', *Catalysts*, vol. 13, no. 1, article 123, https://doi.org/10.3390/catal13010123

da Trindade, LG, Assis, M, Souza, JC, Trench, AB, Núñez-de la Rosa, Y, Teodoro, MD, Schwanke, AJ, Longo, E, Perrechil, F & Braga, ARCB 2024, 'Improving the photocatalytic dye degradation performance and bactericidal properties of Brazilian Amazon kaolin-waste by adding ZnO and Ag₃PO₄', *Journal of Alloys and Compounds*, vol. 971, article 172556, https://doi.org/10.1016/j.jallcom.2023.172556

da Trindade, LG, Hata, GY, Souza, JC, Soares, MRS, Leite, ER, Pereira, EC, Longo, E & Mazzo, TM 2019, 'Preparation and characterization of hematite nanoparticles–decorated zinc oxide particles (ZnO/Fe_2O_3) as photoelectrodes for solar cell applications', *Journal of Materials Science*, vol. 55, pp. 2923–2936, https://doi.org/10.1007/s10853-019-04135-x

Darmadi, Lubis, MR, Masrura, M, Syahfatra, A & Mahidin 2023, 'Clay and zeolite-clay based monoliths as adsorbents for the Hg(II) removal from the aqueous solutions', *International Journal of Technology*, vol. 14, no. 1, pp. 129–141, https://doi.org/10.14716/ijtech.v14i1.5134

Groeneveld, I, Kanelli, M, Ariese, F & van Bommel, MR 2023, 'Parameters that affect the photodegradation of dyes and pigments in solution and on substrate – An overview', *Dyes and Pigments*, vol. 210, article 110999, https://doi.org/10.1016/j.dyepig.2022.110999

Hakimi, B, Ghorbanpour, M & Feizi, A 2018, 'ZnO/bentonite nanocomposites prepared with solid–state ion exchange as photocatalysts', *Journal of Ultrafine Grained and Nanostructured Materials*, vol. 51, no. 2, pp. 139–146, https://doi.org/10.22059/jufgnsm.2018.02.05

Hamrayev, H & Shameli, K 2022, 'Synthesis and characterization of ionically cross-linked chitosan nanoparticles', *Journal of Research in Nanoscience and Nanotechnology*, vol. 7, no. 1, pp. 7–13, https://doi.org/10.37934/jrnn.7.1.713

Hariyanto, B, Wardani, DAP, Kurniawati, N, Har, NP, Darmawan, N & Irzaman 2021, 'X-ray peak profile analysis of silica by Williamson–Hall and size–strain plot methods', *Journal of Physics: Conference Series*, vol. 2019, no. 1, article 012106, https://doi.org/10.1088/1742-6596/2019/1/012106

Heriyanto, H, Muraza, O, Nasser, GA, Sanhoob, MA, Bakare, IA, Budhijanto, Rochmadi, Wijaya, K & Budiman, A 2023, 'Improvement of catalyst activity in methanol–to–olefin conversion via metal (Sr/La) impregnation over ZSM–5 catalyst', *International Journal of Technology*, vol. 14, no. 1, pp. 142–151, https://doi.org/10.14716/ijtech.v14i1.4884

Holmberg, BA, Wang, H & Yan, Y 2004, 'High silica zeolite Y nanocrystals by dealumination and direct synthesis', *Microporous and Mesoporous Materials*, vol. 74, no. 1–3, pp. 189–198, https://doi.org/10.1016/j.micromeso.2004.06.018

Ivanić, M, Vdović, N, de Brito Barreto, S, Bermanec, V & Sondi, I 2015, 'Mineralogy, surface properties and electrokinetic behaviour of kaolin clays derived from naturally occurring pegmatite and granite deposits', *Geologia Croatica*, vol. 68, no. 2, pp. 139–145, https://doi.org/10.4154/gc.2015.09

Janíková, B, Tokarský, J, Kutláková, KM, Kormunda, M & Neuwirthová, L 2017, 'Photoactive and non–hazardous kaolin/ZnO composites prepared by calcination of sodium zinc carbonate', *Applied Clay Science*, vol. 143, pp. 345–353, https://doi.org/10.1016/j.clay.2017.04.003

Kamaluddin, MR, Zamri, NII, Kusrini, E, Prihandini, WW, Mahadi, AH & Usman, A 2021, 'Photocatalytic activity of kaolin–titania composites to degrade methylene blue under UV light irradiation; kinetics, mechanism and thermodynamics', *Reaction Kinetics, Mechanisms and Catalysis*, vol. 133, no. 1, pp. 517–529, https://doi.org/10.1007/s11144–021–01986–x

Kusrini, E, Rafdi, AR, Usman, A, Wilson, LD, Degirmenci, V, Abdullah, MAA & Sofyan, N 2024, 'Performance comparison of heterogeneous catalysts based on natural Bangka kaolin for biodiesel production by acid and base activation processes', *International Journal of Technology*, vol. 15, no. 6, pp. 1994–2008, https://doi.org/10.14716/ijtech.v15i6.7023

Kutláková, KM, Tokarský, J & Peikertová, P 2015, 'Functional and eco–friendly nanocomposite kaolinite/ZnO with high photocatalytic activity', *Applied Catalysis B: Environmental*, vol. 162, pp. 392–400, https://doi.org/10.1016/j.apcatb.2014.07.018

- Li, C, Dong, X, Zhu, N, Zhang, X, Yang, S, Sun, Z, Liu, Y, Zheng, S & Dionysiou, DD 2020, 'Rational design of efficient visible–light driven photocatalyst through 0D/2D structural assembly: Natural kaolinite supported monodispersed TiO₂ with carbon regulation', *Chemical Engineering Journal*, vol. 396, article 125311, https://doi.org/10.1016/j.cej.2020.125311
- Li, T, Xiao, K, Yang, B, Peng, G, Liu, F, Tao, L, Chen, S, Wei, H, Yu, G & Deng, S 2019, 'Recovery of Ni(II) from real electroplating wastewater using fixed–bed resin adsorption and subsequent electrodeposition', *Frontiers of Environmental Science and Engineering*, vol. 13, no. 6, pp. 1–12, https://doi.org/10.1007/s11783-019-1175-7

Madani, H, Wibowo, A, Sasongko, D, Miyamoto, M, Uemiya, S & Budhi, YW 2024, 'Novel multiphase CO₂ photocatalysis system using N–TiO₂/CNCs and CO₂ nanobubble', *International Journal of Technology*, vol. 15, no. 2, pp. 432–441, https://doi.org/10.14716/ijtech.v15i2.6694

Maged, A, Ismael, IS, Kharbish, S, Sarkar, B, Peräniemi, S & Bhatnagar, A 2020, 'Enhanced interlayer trapping of Pb(II) ions within kaolinite layers: Intercalation, characterization, and sorption studies', *Environmental Science and Pollution Research*, vol. 27, no. 2, pp. 1870–1887, https://doi.org/10.1007/s11356-019-06845-w

Majid, AFA, Dewi, R, Shahri, NNM, Shahrin, EWES, Kusrini, E, Shamsuddin, N, Lim, JW, Thongratkaew, S, Faungnawakij, K & Usman, A 2023, 'Enhancing adsorption performance of alkali activated kaolinite in the removal of antibiotic rifampicin from aqueous solution', *Colloids and Surfaces A: Physicochemical and Engineering Aspects*, vol. 676, article 132209, https://doi.org/10.1016/j.colsurfa.2023.132209

Mousavi, M, Habibi–Yangjeh, A & Abitorabi, M 2016, 'Fabrication of novel magnetically separable nanocomposites using graphitic carbon nitride, silver phosphate and silver chloride and their applications in photocatalytic removal of different pollutants using visible–light irradiation', *Journal of Colloid and Interface Science*, vol. 480, pp. 218–231, https://doi.org/10.1016/j.jcis.2016.07.021

Mustapha, S, Tijani, JO, Ndamitso, MM, Abdulkareem, SA, Shuaib, DT, Mohammed, AK & Sumaila, A 2020, 'The role of kaolin and kaolin/ZnO nanoadsorbents in adsorption studies for tannery wastewater treatment', *Scientific Reports*, vol. 10, no. 1, article 13068, https://doi.org/10.1038/s41598-020-69808-z

Nugrahaningtyas, KD, Heraldy, E, Rachmadani, Hidayat, Y & Kartini, I 2021, 'Effect of synthesis and activation methods on the character of CoMo/ultrastable Y–zeolite catalysts', *Open Chemistry*, vol. 19, no. 1, pp. 745–754, https://doi.org/10.1515/chem-2021-0064

Nugrahaningtyas, KD, Kurniawati, MF, Masykur, A & Quratul'aini, NA 2022, 'Periodic trends in the character of first–row transition metals–based catalysts embedded on mordenite', *Moroccan Journal of Chemistry*, vol. 10, no. 3, pp. 375–386, https://doi.org/10.48317/IMIST.PRSM/morjchem-v10i3.32665

Nugrahaningtyas, KD, Kusrini, E, Salsabila, S, Fitriana, D, Usman, A, Kusumaningsih, T & Santoso, SJ 2025, 'Synthesis of transition metal–nanochitosan composites using Ni, Cu, Zn, and Ag metal ions and applications as antibacterial agents', *International Journal of Technology*, vol. 16, no. 1, pp. 207–220, https://doi.org/10.14716/jitech.v16i1.6969

Pal, S, Dixit, S & Lal, S 2016, 'Synthesis and characterization of cation exchange PVA-g-PAA/PBI sulfone membrane for the electrolysis of sodium chloride', *Journal of Membrane Science and Research*, vol. 2, no. 3, pp. 147–154, https://doi.org/10.22079/JMSR.2016.20313

Ramadji, C, Messan, A, Sore, SO, Prud'homme, E & Nshimiyimana, P 2022, 'Microstructural analysis of the reactivity parameters of calcined clays', *Sustainability*, vol. 14, no. 4, article 2308, https://doi.org/10.3390/su14042308

Ramakrishna, S, Kusrini, E, Nurhayati, RW & Whulanza, Y 2023, 'Advancing green growth through innovative engineering solutions', *International Journal of Technology*, vol. 14, no. 7, pp. 1402–1407, https://doi.org/10.14716/ijtech.v14i7.6869

Santos, PB, Dos Santos, HF & Andrade, GFS 2021, 'Photodegradation mechanism of the RB5 dye: A theoretical and spectroscopic study', *Journal of Photochemistry and Photobiology A: Chemistry*, vol. 416, article 113315, https://doi.org/10.1016/j.jphotochem.2021.113315

Seo, O, Tayal, A, Kim, J, Song, C, Chen, Y, Hiroi, S, Katsuya, Y, Ina, T, Sakata, O, Ikeya, Y, Takano, S, Matsuda, A & Yoshimoto, M 2019, 'Tuning of structural, optical band gap, and electrical properties of room–temperature–grown epitaxial thin films through the Fe₂O₃:NiO ratio', *Scientific Reports*, vol. 9, no. 1, article 4304, https://doi.org/10.1038/s41598–019–41049–9

Shao, GN, Engole, M, Imran, SM, Jeon, SJ & Kim, HT 2015, 'Sol–gel synthesis of photoactive kaolinite–titania: Effect of the preparation method and their photocatalytic properties', *Applied Surface Science*, vol. 331, pp. 98–107, https://doi.org/10.1016/j.apsusc.2014.12.199

Sudha, M, Saranya, A, Selvakumar, G & Sivakumar, N 2014, 'Microbial degradation of azo dyes: A review', *International Journal of Current Microbiology and Applied Sciences*, vol. 3, no. 2, pp. 670–690, http://www.ijcmas.com/vol-3-2/M.Sudha,%20et%20al.pdf

Suhaimi, NAA, Shahri, NNM, Samat, JH, Kusrini, E, Lim, JW, Hobley, J & Usman, A 2022, 'Domination of methylene blue over rhodamine B during simultaneous photocatalytic degradation by TiO_2 nanoparticles in an aqueous binary solution under UV irradiation', *Reaction Kinetics, Mechanisms and Catalysis*, vol. 135, no. 1, pp. 511–527, https://doi.org/10.1007/s11144-021-02098-2

Tsaviv, JN, Eneji, IS, Shato'Ato, R, Ahemen, I, Jubu, PR & Yusof, Y 2024, 'Photodegradation, kinetics and non–linear error functions of methylene blue dye using SrZrO₃ perovskite photocatalyst', *Heliyon*, vol. 10, no. 14, article e34517, https://doi.org/10.1016/j.heliyon.2024.e34517

Türkyılmaz, ŞŞ, Güy, N & Özacar, M 2017, 'Photocatalytic efficiencies of Ni, Mn, Fe and Ag doped ZnO nanostructures synthesized by hydrothermal method: The synergistic/antagonistic effect between ZnO and metals', *Journal of Photochemistry and Photobiology A: Chemistry*, vol. 341, pp. 39–50, https://doi.org/10.1016/j.jphotochem.2017.03.027

Ulfa, M, Pertiwi, YE, Saraswati, TE, Bahruji, H & Holilah, H 2023, 'Synthesis of iron triad metals–modified graphitic mesoporous carbon for methylene blue photodegradation', *South African Journal of Chemical Engineering*, vol. 45, pp. 149–161, https://doi.org/10.1016/j.sajce.2023.05.008

Ulfiati, R, Dhaneswara, D, Harjanto, S & Fatriansyah, JF 2022, 'Synthesis and characterization ZSM–5 based on kaolin as a catalyst for catalytic cracking of heavy distillate', *International Journal of Technology*, vol. 13, no. 4, pp. 860–869, https://doi.org/10.14716/ijtech.v13i4.5150

Wang, J, Fu, L, Yang, H, Zuo, X & Wu, D 2021, 'Energetics, interlayer molecular structures, and hydration mechanisms of dimethyl sulfoxide (DMSO)–kaolinite nanoclay guest–host interactions', *Journal of Physical Chemistry Letters*, vol. 12, no. 40, pp. 9973–9981, https://doi.org/10.1021/acs.jpclett.1c02729

Wang, X, Jiang, J & Gao, W 2022, 'Reviewing textile wastewater produced by industries: Characteristics, environmental impacts, and treatment strategies', *Water Science & Technology*, vol. 85, no. 7, pp. 2076–2096, https://doi.org/10.2166/wst.2022.088

Wongso, V, Chen, CJ, Razzaq, A, Kamal, NA & Sambudi, NS 2019, 'Hybrid kaolin/TiO₂ composite: Effect of urea addition towards an efficient photocatalyst for dye abatement under visible light irradiation', *Applied Clay Science*, vol. 180, article 105158, https://doi.org/10.1016/j.clay.2019.105158

Wulandari, DA, Zulys, A & Kusrini, E 2019, 'Samarium complexes from 2,6-naphtalenedicarboxylate: Synthesis, photocatalytic properties and degradation of methylene blue', *IOP Conference Series: Materials Science and Engineering*, vol. 546, article 042050, https://doi.org/10.1088/1757-899X/546/4/042050

Yahaya, S, Jikan, SS, Badarulzaman, NA & Adamu, AD 2017, 'Chemical composition and particle size analysis of kaolin', *Path of Science*, vol. 3, no. 10, pp. 1001–1004, https://doi.org/10.22178/pos.27-1

Zagloel, TYM, Harwahyu, R, Maknun, IJ, Kusrini, E & Whulanza, Y 2023, 'Developing models and tools for exploring the synergies between energy transition and the digital economy', *International Journal of Technology*, vol. 14, no. 8, pp. 1615–1622, https://doi.org/10.14716/ijtech.v14i8.6906

Zamri, NII, Zulmajdi, SLN, Daud, NZA, Mahadi, AH, Kusrini, E & Usman, A 2021, 'Insight into the adsorption kinetics, mechanism, and thermodynamics of methylene blue from aqueous solution onto pectinalginate-titania composite microparticles', *SN Applied Sciences*, vol. 3, no. 2, article 222, https://doi.org/10.1007/s42452-021-04245-9

Zhang, Y, Zhao, X, Shang, B, Wang, X, Wu, X & Li, T 2024, 'Characterization of nano-kaolin and its enhancement of the mechanical and corrosion resistance of epoxy coatings', *Materials Today Communications*, vol. 41, article 110371, https://doi.org/10.1016/j.mtcomm.2024.110371

Zulmajdi, SLN, Zamri, NII, Yasin, HM, Kusrini, E, Hobley, J & Usman, A 2019, 'Comparative study on the adsorption, kinetics, and thermodynamics of the photocatalytic degradation of six different synthetic dyes on TiO_2 nanoparticles', *Reaction Kinetics, Mechanisms and Catalysis*, vol. 129, no. 1, pp. 519–534, https://doi.org/10.1007/s11144-019-01701-x

Zyoud, AH, Zubi, A, Zyoud, SH, Hilal, MH, Zyoud, S, Qamhieh, N, Hajamohideen, AR & Hilal, HS 2019, 'Kaolin–supported ZnO nanoparticle catalysts in self–sensitized tetracycline photodegradation: Zero-point charge and pH effects', *Applied Clay Science*, vol. 182, article 105294, https://doi.org/10.1016/j.clay.2019.105294